Linear reciprocating wear of yttria stabilized zirconia based composite coatings developed by thermal spray

Nath, S., Manna, I., Lawrence, J. & Dutta Majumdar, J.

Original citation & hyperlink:
Nath, S, Manna, I, Lawrence, J & Dutta Majumdar, J 2020, 'Linear reciprocating wear of yttria stabilized zirconia based composite coatings developed by thermal spray', Journal of Materials Engineering and Performance, vol. 29, no. 8, pp. 5041–5056.
https://dx.doi.org/10.1007/s11665-020-05039-7

DOI 10.1007/s11665-020-05039-7
ISSN 1059-9495
ESSN 1544-1024

Publisher: Springer

The final publication is available at Springer via http://dx.doi.org/10.1007/s11665-020-05039-7

Linear reciprocating wear of yttria stabilized zirconia based composite coatings developed by thermal spray

Subhasisa Nath[a*], Indranil Manna[b], Jonathan Lawrence[a], Jyotsna Dutta Majumdar[b]

[a]School of Mechanical, Aerospace and Automotive Engineering, Coventry University, Coventry, CV1 2JH, United Kingdom
[b]Department of Metallurgical and Materials Engineering, Indian Institute of Technology, Kharagpur, West Bengal, 721302, India

Abstract:

Ceramic matrix composites (CMCs) are the preferred material for high temperature application due to their low density, improved strength and toughness, and high temperature capabilities. In the present study, we report the kinetics and mechanism of linear reciprocating wear of yttria stabilized zirconia (YSZ) based composite coatings developed by thermal spray technique. Composite coatings with different volume fractions of CoNiCrAlY and YSZ phases were subjected to linear reciprocating wear under an applied normal load of 10 N against a WC counter-body. The kinetics of wear was investigated by measuring the wear depth over time of coated components against WC surface. Adhesive wear in the 100% CoNiCrAlY coating was responsible for increased friction in the coating which changed to a three-body abrasion in the case of 100% YSZ coating. The composition coatings had a significant effect on the wear mechanism with the ceramic coatings were fractured under reciprocating load. Microcrack propagation and fracturing of ceramic splats were the dominant modes of wear in the ceramic coatings. The 100% YSZ coating showed significant wear than 100% CoNiCrAlY and 50% YSZ + 50% CoNiCrAlY coatings. The mode of wear changed with the presence of a metallic phase in the 50% YSZ + 50% CoNiCrAlY coating. The mode of wear was further studied by the detailed microstructural observation of worn track and correlating it with the wear kinetics and coefficient of friction.

Keywords: CMCs; Coating; Thermal spray; Linear reciprocating wear; Hardness

*Corresponding author: subhasisa.nath@coventry.ac.uk

1. Introduction

Oxide ceramics are drawing attention in the manufacturing industries owing to their high hardness, chemical inertness, low thermal conductivity *etc* [1]. However, these ceramic materials have inferior strength and poor toughness [1,2]. Among the oxide ceramics, yttria stabilized zirconia (YSZ) and alumina (Al_2O_3) possess many technological advantages over other ceramics due to high hardness, high

strength, superior fracture toughness, excellent wear resistance, high chemical and corrosion resistance, and excellent biocompatibility [3–6]. The loss of material due to wear and energy loss due to friction can be minimized by keeping the coefficient of friction as low as possible. Despite the widespread use of YSZ as a heat resistant material, it lacks the strength required to be used for wear resistant material such as in applications involving cutting tool and bio-implants [7–11]. On the other hand, Al_2O_3 possesses the necessary hardness sought for the wear resistance application, but it underperforms due to inferior fracture toughness [12]. On the other hand, a multi-component ceramic structure has been beneficial in improving strength and toughness [13–17]. The addition of a second phase, in the form of fiber or whisker, to the ceramic matrix has been beneficial in increasing the mechanical properties of ceramic coatings due to different mechanisms such as whisker pullout, crack deflection, whisker–matrix interface delamination, whisker breakage, and matrix fracture mechanisms [18–21]. Composites of YSZ and Al_2O_3 showed maximum wear resistance due to the combined effect of high hardness and high fracture toughness [14,22]. The reported literature on the quantity of second phase addition to the Al_2O_3/YSZ composite to improve the mechanical and wear properties were not consistent [14,23–25]. The wear resistance of the Al_2O_3/YSZ composites, with 80% YSZ, was measured to be 4 -10 times that of the monolithic YSZ ceramics [24].

The mechanism involved in the wear of coatings is governed by its hardness, fracture toughness, microstructure, porosity content, presence of microcracks, phases present, residual stress etc. The wear resistance of the monolithic coatings has been improved by grain size reduction, doping and adding a second phase to the matrix to form a composite [26–29]. The wear rate of nanostructured YSZ coating was less than one-fourth of wear rate of conventional coating [30]. Reduction in the micrometer-sized defects, microcrack toughening, phase transformation toughening, enhanced inter-splat bonding, increased hardness due to the reduction in grain size in nanostructured YSZ coatings were the mechanisms responsible for the improved wear performance of nano-structured thermal barrier coatings (TBCs) than the conventional TBCs [31–34].

The thermal spray deposition has been the preferred technique to deposit ceramic coatings due to its ability to melt the high melting point oxide and non-oxide ceramics [35]. Many reported studies used air plasma spray to deposit Al_2O_3, YSZ, CoNiCrAlY based composite coatings [22,29,36–39]. However, most of the studies carried out on these thermal spray composite coatings were subjected to either erosion wear or sliding wear [26–29,37–39]. The erosion wear of CoNiCrAlY-YSZ composite coating was studied by Ramanujam and Nakamura [39]. The solid particle erosion wear resistance was significantly increased due to the presence of tougher CoNiCrAlY metallic phase in the composite coating. There are no available reports on linear reciprocating wear study of CoNiCrAlY-YSZ composite coating. The wear resistance of the YSZ-Al_2O_3 composite coatings was significantly higher than YSZ or Al_2O_3 coating alone as YSZ-Al_2O_3 composite coatings exhibit high hardness and high fracture toughness [22,29,38,40–42]. The hardness of the YSZ-Al_2O_3 composite coating increased with the addition of Al_2O_3 and the presence of YSZ in the composite coating improves the fracture toughness [41,42]. Liang *et al* [29] reported that the mechanism of wear changes with the transition of the coefficient of friction during the wear process. In the onset of wear, the wear process was mild and the main wear mechanism was ploughing which changed to the interfacial fatigue and abrasive wear. In the later stage, the wear was severe.

The reported wear studies were primarily based on the sliding and erosive wear properties evaluation of monolithic and composite ceramic coatings with the studies on the linear reciprocating wear of the YSZ based composite coatings are scarce [22,26,39,27,28,30–34,36]. In the present study, a detailed investigation on the wear and friction behavior of the YSZ, CoNiCrAlY, Al_2O_3 monolithic coatings as well as of their composite coatings have been investigated using linear reciprocating wear test. The use of YSZ, Al_2O_3 and CoNiCrAlY as the constituent phases in the composite coatings was to evaluate the efficacy of the composite coating systems against linear reciprocating wear. The kinetics and mechanism of wear have been proposed through a detailed analysis of the microstructures of the worn-out surface.

2. Experimental

2.1. Feedstock materials

In the present study, commercially available spherical YSZ (7 wt% Y_2O_3-ZrO_2, Amperit 831.007, particle size 15–85 µm) ceramic powder, irregular shaped Al_2O_3 (Amperit 740.1, particle size 22–45 µm) ceramic powder and spherical CoNiCrAlY alloy powder (Co-32Ni-21Cr-8Al-0.5Y in wt%, MEC 9950AM, particle size 15–45 µm) were used as feedstock powders. The details of the phase composition and microstructure of the feedstock powders were shown elsewhere [43]. To form composite coatings, the feedstock powders were premixed in the volume ratio of 70:30, 50:50, and 30:70 using a planetary ball mill for 4 h at 300 rpm to ensure proper mixing of powders without altering their original shapes.

2.2. Coating processing

In the present study, Inconel 718 superalloy (compositions: Ni-18.8Fe-14Cr-7.3Nb-1.7Mo-1.3Ti-0.7Al in wt.%) was used as the substrate for thermal spray deposition. Initially, CoNiCrAlY powder was deposited onto the sandblasted and cleaned Inconel 718 superalloy substrates using high velocity oxy-fuel spray (HVOF) as a bond coat. For the development of duplex coating, YSZ powder was sprayed onto the bond coated surface using an 80 kW atmospheric plasma spray system (SG 100, Miller Thermal Inc. USA). For the development of composite coatings, premixed CoNiCrAlY and YSZ, CoNiCrAlY and Al_2O_3, and Al_2O_3 and YSZ powders in different volume ratio were plasma sprayed onto the bond coated substrate. The graded coating was developed by depositing premixed powders with varying composition in a layer by layer manner. Table 1 summarizes the thermal spray process parameters employed for the deposition of composite coatings. The process parameters were optimized for all composite coating layers taking into account their composition.

Table 1 Thermal spray process parameters employed in the present study

Air plasma spray (APS)		High velocity oxy-fuel spray (HVOF)	
D.C voltage (V)	46	Fuel gas	LPG (Industry grade)
D.C current (A)	650	Fuel gas flow rate, slpm*	250
Argon gas flow rate (primary), slpm*	36	Fuel gas pressure, bar	60
Argon gas pressure (primary), psi	120	Oxygen flow rate, slpm*	10
Hydrogen gas flow rate (secondary), slpm*	5	Oxygen pressure, bar	7
Hydrogen gas pressure (secondary), psi	58	Oxygen/Fuel ratio	4.3
Carrier gas (Argon) flow rate, slpm*	5.1	Powder feed rate, g/min	25
Carrier gas (Argon) Pressure, psi	3.8	Standoff distance, mm	280
Powder feed rate, g/min	21	Spray angle	90°
Standoff distance, mm	90		
Spray angle	90°		
**slpm: standard lire per minute*			

2.3. Characterization of composite coatings

A detailed characterization of the microstructure and composition of the composite coatings was carried out by field emission gun scanning electron microscopy (SUPRA 40, Zeiss SMT AG, Germany) equipped with energy dispersive X-ray spectroscopy (EDS). X-ray diffraction (XRD; Bruker D8 Discover, Germany) analysis of the composite coatings was conducted using Cu Kα radiation (wavelength ~ 0.15418 nm) at a scanning speed of 0.05°/s to investigate the phases formed on the composite coatings' surface. The X-ray source was kept at an accelerating voltage of 40 kV and a current of 40 mA. For the

characterization of composite coatings, each composite coating layer was developed and analysed individually.

Porosities of the freestanding composite coatings were measured using the Archimedes' principle as explained elsewhere [43].

2.4. Thermal property measurement

The coefficient of thermal expansion (CTE) of the individual freestanding composite coating (with a dimension of $10 \times 5 \times 1$ mm^3) in as-sprayed condition was measured in air from 300 K to 1273 K using a dilatometer (NETZSCH DIL 402 C, Germany) at a heating rate of 10 K/min. The fractional change in length, $\Delta L/L$ as a function of temperature was measured and the coefficients of thermal expansion, α, was measured from the slope of the curve.

Thermal diffusivity of the individual free-standing composite coating ($10 \times 10 \times 1$ mm^3) was measured using laser flash technique (LFA 427, Netschz, Germany) from 300 K to 1273 K under N_2 atmosphere. The surface of the composite coatings was coated with colloidal graphite before the laser flash test for uniform absorption and emission of laser energy. The pulsed width is chosen to be 0.5 ms and the radiation model was used for calculation of thermal conductivity.

2.5. Mechanical property measurement

The hardness of the coating (both on the top surface and along the cross-section) was measured using Vickers microhardness tester (UHL-VMHT 001, Germany) with a 200 *gf* applied load. The hardness values were reported in Vickers hardness number (VHN).

Nanoindentation tests were carried out on the cross-section of the composite coatings using a nanoindenter (Hysitron-TI950 Triboindentor) with a Berkovich tip (tip radius <150 nm) at a maximum load of 8 mN. The details of the process were explained elsewhere [44].

2.6. Linear reciprocating wear test

Linear reciprocating wear tests were performed with a ball-on-plate type wear tester (DUCOM: TR-283M-M4, India) using 6 mm diameter WC ball as the counter-body against the coating's top surface at ambient temperature (295–298 K) and humidity (50–55%). The wear tests were carried out for 30 minutes under a normal load of 10 N and with a constant frequency of 10 Hz and a constant displacement stroke of 1 mm. To reduce the measurement error, the tests were repeated for 4 times and an average of the test values was reported. Following the wear test, a detailed investigation of the worn-out surface was carried out by scanning electron microscopy (SUPRA 40, Zeiss SMT AG, Germany) to establish the mechanism of wear.

3. Results & discussion

3.1. Microstructural investigation

Fig. 1 shows the scanning electron micrographs of the cross-section of (a) YSZ-CoNiCrAlY duplex coating, (b) YSZ-CoNiCrAlY composite coating, (c) CoNiCrAlY/Al_2O_3/YSZ composite coating, and (d) high magnification view of 100% YSZ coating. Presence of microstructural defects such as globular porosities/voids, intra-lamellar cracks, inter-lamellar porosities was evident from the topcoat microstructure of all the coating systems. The source of these microstructural defects was from poor inter-splat bonding, improper melting of powder particles during plasma spraying, and plasma gas/carrier gas entrapment in the coating [45–47]. Fig. 1(d) shows the formation of vertical cracks in the YSZ coating (marked by arrows) due to the development of tensile stress in the splats during rapid solidification of molten splats.

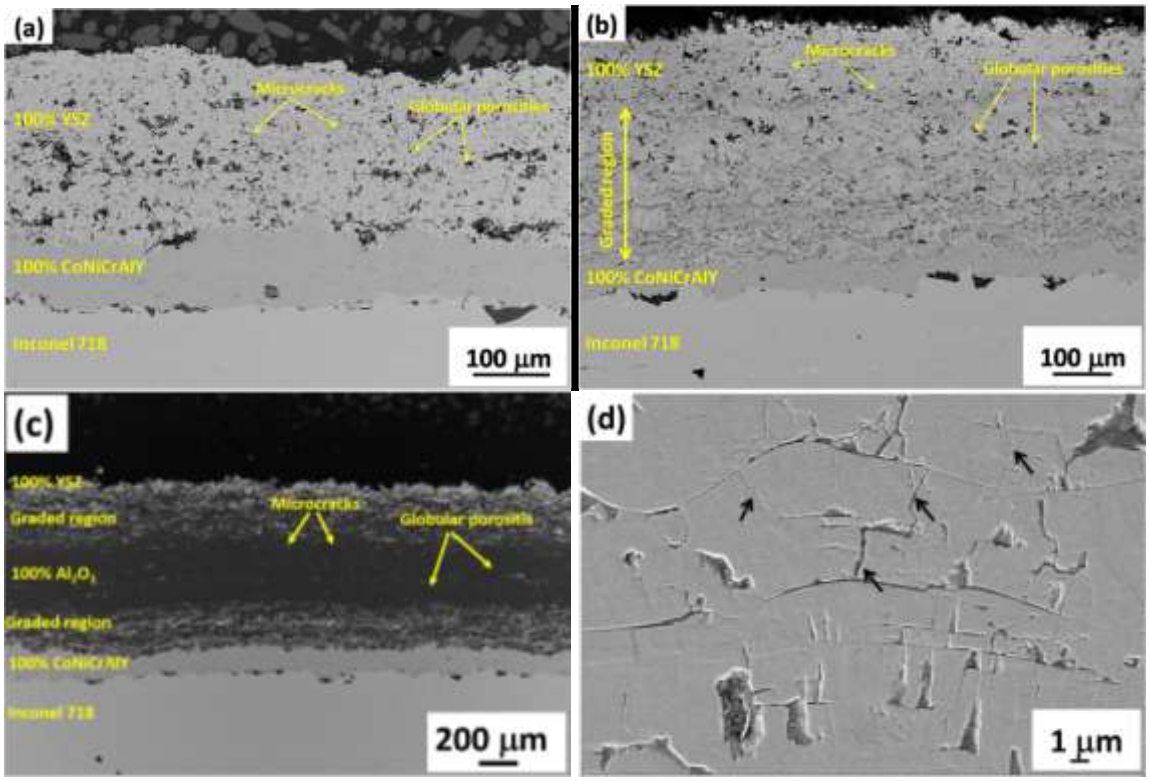

Fig. 1 Microstructure of cross-section of (a) duplex YSZ-CoNiCrAlY coating, (b) YSZ-CoNiCrAlY composite coating (c) CoNiCrAlY/Al_2O_3/YSZ composite coating, and (d) high magnification view of 100% YSZ coating.

Fig. 2 shows the X-ray diffraction (XRD) scans of (a) YSZ-CoNiCrAlY composite coatings, (b) YSZ-Al_2O_3 composite coatings, and (c) Al_2O_3-CoNiCrAlY composite coatings. The XRD scan of the top surface of 100% YSZ coating (plot 1) showed the formation of non-transformable tetragonal zirconia (t′-ZrO_2) as the only major phase in Fig. 2 (a). The formation of t′-ZrO_2 phase on the surface of 100% YSZ coating was reported to improve the mechanical integrity of the coating [48]. The XRD scans of YSZ and CoNiCrAlY composite coatings showed the formation of t′-ZrO_2, γ-Co and β-CoAl phases as shown in Fig. 2 (a). The XRD scans of the YSZ and Al_2O_3 composite coatings showed the formation of t′-ZrO_2, α-Al_2O_3 and γ-Al_2O_3 phases as shown in Fig. 2 (b). Similarly, the XRD scans of Al_2O_3 and CoNiCrAlY composite coatings showed the formation of α-Al_2O_3, γ-Al_2O_3, γ-Co and β-CoAl phases as shown in Fig. 2 (c).

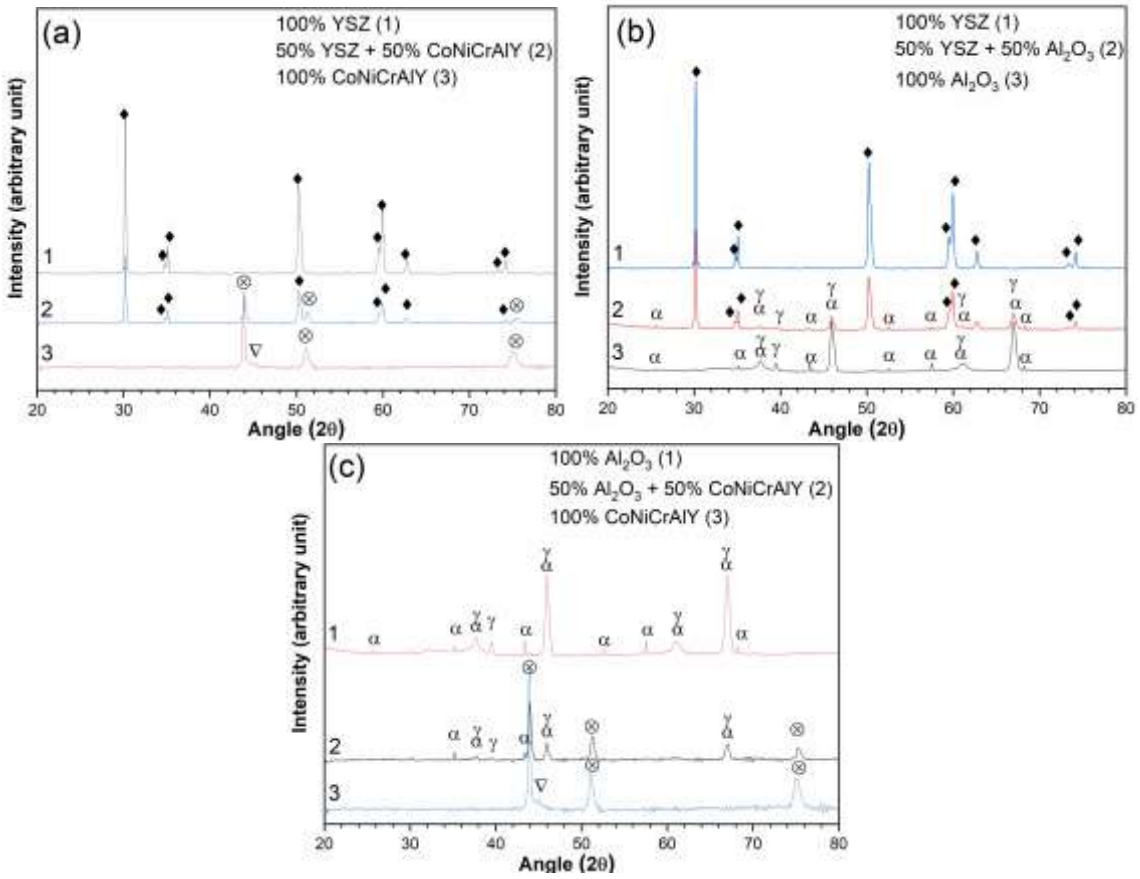

Fig. 2 X-ray diffraction scans of (a) YSZ-CoNiCrAlY composite coatings, (b) YSZ-Al_2O_3 composite coatings, and (c) Al_2O_3-CoNiCrAlY composite coatings. (♦ t′-ZrO_2; ⊗ ϒ-Co (Matrix); α Al_2O_3 (Trigonal); γ Al_2O_3 (Cubic); ∇ β-CoAl)

Table 2 shows the characteristics of composite coating layers. The porosity contents in the YSZ-CoNiCrAlY, YSZ-Al_2O_3 and Al_2O_3-CoNiCrAlY composite coatings are presented in Table 2. The porosity content in YSZ-CoNiCrAlY composite coatings decreased with the increase in the CoNiCrAlY content in the composite coating. A similar trend in the porosity content in Al_2O_3-CoNiCrAlY composite coatings can be seen in Table 2. However, the porosity content in the YSZ-Al_2O_3 composite coatings showed no specific trend with composition. The decreased porosities of YSZ-CoNiCrAlYand Al_2O_3-CoNiCrAlY composite coatings with the increase in the CoNiCrAlY content was due to proper bonding between the splats as a result of increased melting of the inflight metallic particles in the plasma jet [43]. A maximum porosity content of 19.6% was measured for the 50% YSZ + 50% Al_2O_3 composite coating and a minimum porosity content of 2.8% was measured for the 100% CoNiCrAlY coating. Table 2

summarizes Young's modulus of the different composite coating layers present in the coating system. The Young's modulus of as-sprayed 100% YSZ coating was measured to vary between 59 GPa and 150 GPa. The wide variation in the value of Young's modulus was reported to be due to the presence of microcracks and fine porosities in the microstructure of plasma sprayed coating which affected the local mechanical properties [44]. The Young's modulus of the 100% CoNiCrAlY coating was measured to be in the range between 150 and 187 GPa. Moreover, Young's modulus in YSZ-CoNiCrAlY composite coatings varied between 59 GPa and 224 GPa including Young's modulus value of the individual composite coating. The measured range in Young's modulus of the composite coatings was due to the contributions from different phases present in the composite coatings. From Table 2, it may be noted that Young's modulus of the composite coating increased with an increase in the CoNiCrAlY phase in the composite coating due to the reduction of porosities and microcracks. The Young's modulus of the composite coating increased with the addition of Al_2O_3 phase in the composite as the Al_2O_3 has high bulk modulus. The thermal conductivity of the YSZ coating was measured to be 0.87 $Wm^{-1}K^{-1}$. The thermal conductivity in YSZ-CoNiCrAlY composite coatings varied from 0.87 $Wm^{-1}K^{-1}$ for 100% YSZ coating to 4.69 $Wm^{-1}K^{-1}$ for 100% CoNiCrAlY coating. On the other hand, in the case of Al_2O_3-CoNiCrAlY and YSZ-Al_2O_3 composite coatings, the thermal conductivity of 100% Al_2O_3 coating was found to be 3.97 $Wm^{-1}K^{-1}$. The thermal conductivities of YSZ-CoNiCrAlY and YSZ-Al_2O_3 composite coatings increased with the increase in the CoNiCrAlY and Al_2O_3 contents, respectively. The coefficient of thermal expansion (CTE) of YSZ-CoNiCrAlY composite coatings increased with the increase in the CoNiCrAlY content in the coating (i.e. 13.1×10^{-6} /K for 100% YSZ coating and 21.2×10^{-6} /K for 100% CoNiCrAlY coating). Similarly, the CTE of YSZ-Al_2O_3 composite coatings decreased with increase in Al_2O_3 content in the coating (i.e. 13.1×10^{-6} /K for 100% YSZ coating and 9.5×10^{-6} /K for 100% Al_2O_3 coating).

Table 2 Summary of characteristics (% porosities, phases present), mechanical (hardness and Young' modulus) and thermal properties (thermal conductivity and CTE) of the composite coatings.

Composite coatings	Thickness, μm	Porosities, %	Phases present	Young's modulus, GPa	Microhardness, VHN	Thermal conductivity at room temperature, $Wm^{-1}K^{-1}$	Coefficient of thermal expansion, 10^{-6} /K
100% YSZ	80 - 250	16	t′- ZrO_2	59 - 150	625 ± 25	0.87	13.1
50% YSZ + 50% CoNiCrAlY	80	4.8	t′- ZrO_2 and γ- Co	150-206	469 ± 20	3.09	16.8
100% CoNiCrAlY	80 - 100	2.8	γ- Co and β- CoAl	150 -187	346 ± 15	4.69	21.7
50% YSZ + 50% Al_2O_3	80	19.5	t′- ZrO_2, α-Al_2O_3 and γ- Al_2O_3	158-186	850 ± 24	1.44	11
100% Al_2O_3	250	13.8	t′- ZrO_2, α-Al_2O_3 and γ- Al_2O_3	109-273	998 ± 26	3.97	9.5
50% Al_2O_3 + 50% CoNiCrAlY	80	3.5	α-Al_2O_3, γ- Al_2O_3 and γ- Co	126-213	515 ± 18	4.02	13.25

3.2. Microhardness distribution

Fig. 3 shows the variation in microhardness with depth from the surface for (a) YSZ-CoNiCrAlY duplex coating, (b) YSZ-CoNiCrAlY composite coating and (c) CoNiCrAlY/Al_2O_3/YSZ composite coating. Fig. 3 (a) shows a nearly stable hardness of 625 VHN up to a depth of 250 μm followed by a decreasing trend up to 350 VHN in the 100% CoNiCrAlY coating. Moreover, the microhardness gradually decreased from 100% YSZ coating to 100% CoNiCrAlY coating in the YSZ-CoNiCrAlY composite coating as shown in Fig. 3 (b). The gradual variation in microhardness is attributed to the graded microstructure of YSZ-CoNiCrAlY composite coating. The gradual variation in composition was reported to improve the overall mechanical integrity of the coating system [49]. In Fig. 3 (c), similar graded variation in microhardness in the CoNiCrAlY/Al_2O_3/YSZ composite coating was measured due to the presence of different phases in the composite coating layers. A maximum microhardness of 1025 VHN was measured for 100% Al_2O_3

layer. Moreover, the microhardness decreased due to lower bulk hardness of YSZ as compared to Al_2O_3 at the outer layer of 100% YSZ coating. The major source of error in the microhardness measurement was mainly from the local variation in material structure due to the presence of porosities and microcracks. These microstructural defects were responsible for a lower microhardness value as compared to its bulk or sintered value. To reduce the measurement errors, five microhardness measurements were carried out under the same conditions which resulted in a standard deviation of below 4%.

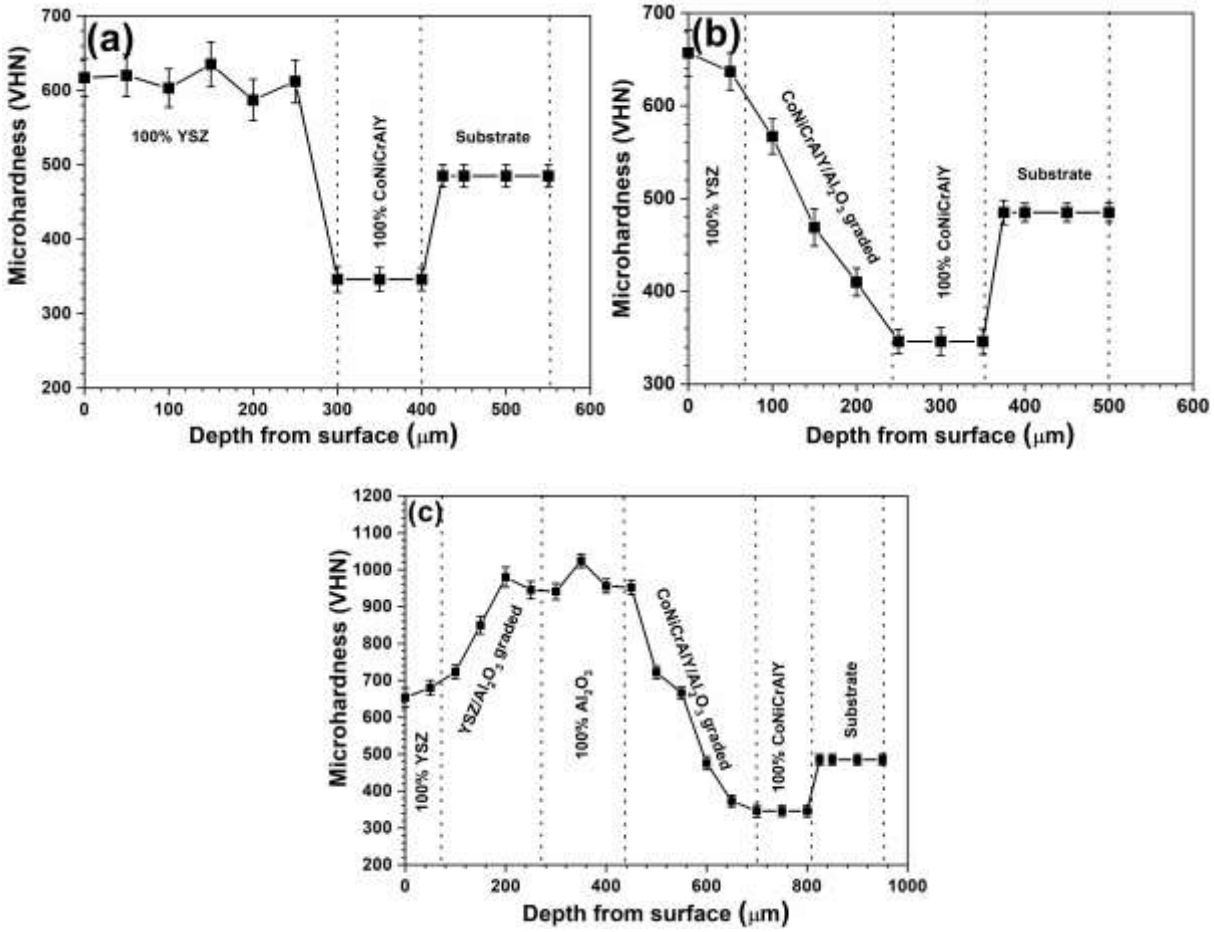

Fig. 3 Variation of microhardness with depth from the surface in (a) duplex YSZ-CoNiCrAlY coating, (b) YSZ-CoNiCrAlY composite coating and (c) CoNiCrAlY/Al_2O_3/YSZ composite coating.

3.3. Wear and friction analysis

YSZ-CoNiCrAlY composite coating system

The depth of wear in the linear reciprocating wear was measured with time. The wear depth signifies the material loss over the time of the test. It may also be considered as a measure of wear resistance of the composite coating with higher wear depth signifies lower resistance to wear. Fig. 4 shows the kinetics of wear in terms of variation of cumulative depth of wear with time for the 100% YSZ coating (plot 1), 50% YSZ + 50% CoNiCrAlY composite coating (plot 2), and 100% CoNiCrAlY coating (plot 3) coatings under a normal load of 10 N load against WC mating surface. Fig. 4 shows a sudden increase in wear depth on the onset of wear for all the coatings followed by the attainment of steady-state wear at a later stage. At the beginning of the wear test, the normal contact pressure was maximum due to the point contact geometry between the WC ball and flat sample. The gradual wear of the WC ball and sample changed the contact geometry to face contact resulting in a decrease in normal pressure. Thus, the wear rate slowed down at the later stage. Wear depth in 100% YSZ coating was measured to be maximum. The poor wear resistance of 100% YSZ coating may be attributed to the presence of several microstructural defects which made the coating prone to fracture due to the abrasive action of WC ball under reciprocating motion. The initial faster rate of wear is attributed to the rapid removal of coating material due to higher contact pressure between the WC ball and the sample's surface. The decreased contact pressure at the later stage slowed down the material removal process thereby decreasing the rate of wear. The reduction in contact pressure along with debris formation at the interface between the WC ball and sample resulted in the attainment of saturation at the final stage of wear. The lowest depth of wear was measured for 100% CoNiCrAlY coating. On the other hand, 50% YSZ + 50% CoNiCrAlY composite coating showed an intermediate wear depth. Hardness plays a key role in tailoring the wear rate of the material with a higher hardness lowers the wear rate of the material. However, a reverse trend was observed in the wear testing of YSZ-CoNiCrAlY composite coating system. In ceramics, the presence of microstructural defects also contributes to the wear rate [50]. In the 100%YSZ coating, the defect density was higher than the 50% YSZ + 50% CoNiCrAlY and 100% CoNiCrAlY composite coatings. The presence of vertical cracks in the 100% YSZ coating (*cf.* Fig. 2(d)) was also responsible for increased

wear depth as the vertical cracks exaggerated the material removal process due to the shear forces acting at the interface between the sample surface and the counter-body under reciprocating motion. The local fluctuations in the wear depth value in Fig. 4 (plot 3) is due to the combined action of reciprocatory motion of the WC ball and the local structure. The microstructure of the composite coatings as shown in Fig. 1 mostly contains micrometer-sized porosities and microcracks. The relative motion between the contact surfaces generated debris due to fracture of splats. The debris formed a triboskin between the contact surfaces which developed localized humps of hard debris resulting in increased fluctuations in the wear depth measurements. The random variations in the wear depth might be caused by different factors. One of the possible ways to minimize the error was to repeat the experiment for multiple times and record the standard deviations. The major sources of error associated with the measurement of wear depth in the case of linear reciprocating wear were wear test parameters (e.g. applied load, frequency, amplitude, relative humidity and temperature), local microstructure (e.g. porosities and microcracks) and local mechanical property (eg. hardness and toughness). The wear tester was calibrated with variations below 1%. However, the microstructure of the composite coatings (*cf*. Fig. 1) was the main source of measurement errors. Thus, a standard deviation of below 10% was measured during the wear test.

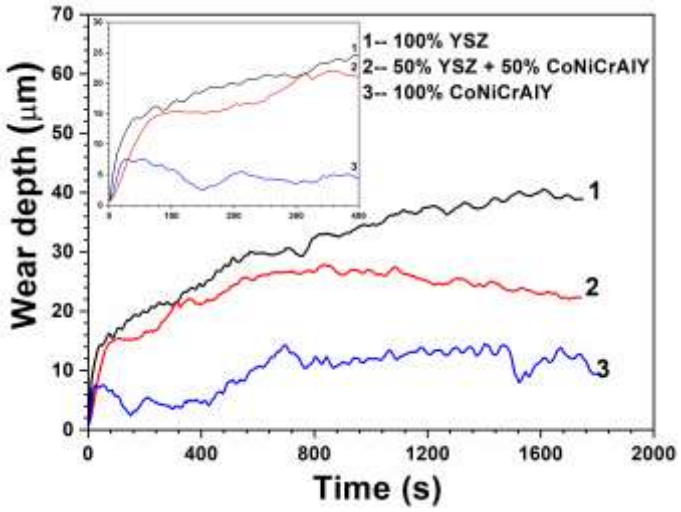

Fig. 4 Variation of wear depth with time in 100% YSZ coating (plot 1), 50% YSZ + 50% CoNiCrAlY composite coating (plot 2) and 100% CoNiCrAlY coating (plot 3) under 10 N load against WC ball. The early stage wear behaviour of the composite coating is shown in the same graph.

Fig. 5 shows the variation of the coefficient of friction (COF) under steady-state with time for the 100% YSZ coating (plot 1), 50% YSZ + 50% CoNiCrAlY composite (plot 2), and 100% CoNiCrAlY coating (plot 3) under the applied normal load of 10 N. A maximum COF (steady-state) of ~ 0.53 was measured for the 100% CoNiCrAlY coating as compared to 100% YSZ coating (~ 0.49) and 50% YSZ + 50% CoNiCrAlY composite coating (~ 0.37) as shown in Fig. 5. Abrasive wear, due to the interaction between the WC counter-body and 100% CoNiCrAlY coating, was the reason behind measured maximum COF (steady-state) in the 100% CoNiCrAlY coating. The COF in 100% YSZ coating showed initial low value as compared to 50% YSZ + 50% CoNiCrAlY composite coating which on later stage exceeded the 50% YSZ + 50% CoNiCrAlY composite coating. The initial low value of COF in 100% YSZ (~ 0.15) coating was due to the adhesive interactions between the two surfaces which on later stage changed to a three-body adhesive wear process due to accumulation of hard particles at the coating and WC counter-body interface.

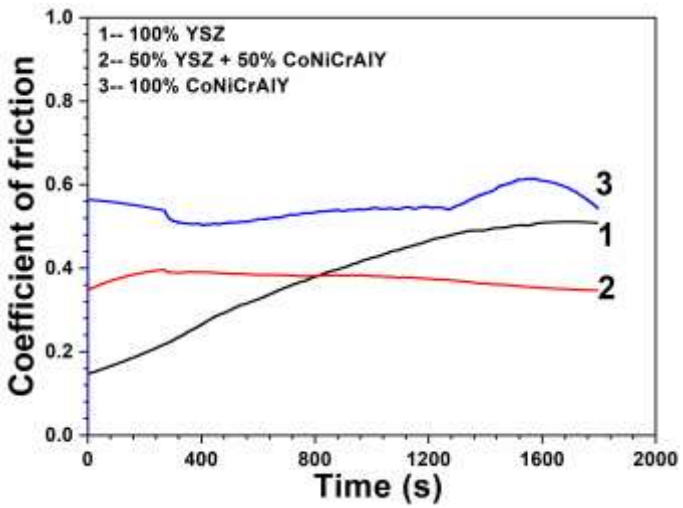

Fig. 5 Variation of COF with time in YSZ coating (plot 1), 50% YSZ + 50% CoNiCrAlY composite coating (plot 2) and 100% CoNiCrAlY coating (plot 3) under 10 N load against WC ball.

YSZ-Al_2O_3 composite coating system

Fig. 6 shows the kinetics of wear in terms of variation of cumulative wear depth with time for the 100% YSZ coating (plot 1), 50% YSZ + 50% Al_2O_3 composite coating (plot 2), and 100% Al_2O_3 coating (plot

3) under the applied normal load of 10 N load against WC mating surface. The wear depth in 100% Al_2O_3 coating was the lowest followed by the 50% YSZ + 50% Al_2O_3 and 100% YSZ coatings as evident from Fig. 6. The superior wear resistance of 100% Al_2O_3 coating is attributed to the high hardness of Al_2O_3 coating as compared to the 50% YSZ + 50% Al_2O_3 and 100% YSZ coatings (*cf.* Fig. 3 (c)). The wear depth of the composite coatings followed a trend with the hardness of the coatings and the 100% YSZ coating showed the highest wear depth due to lower hardness as compared to other coatings. Fluctuations in the wear plots were due to reciprocating action of mating surface which caused the repeated application and release of loads.

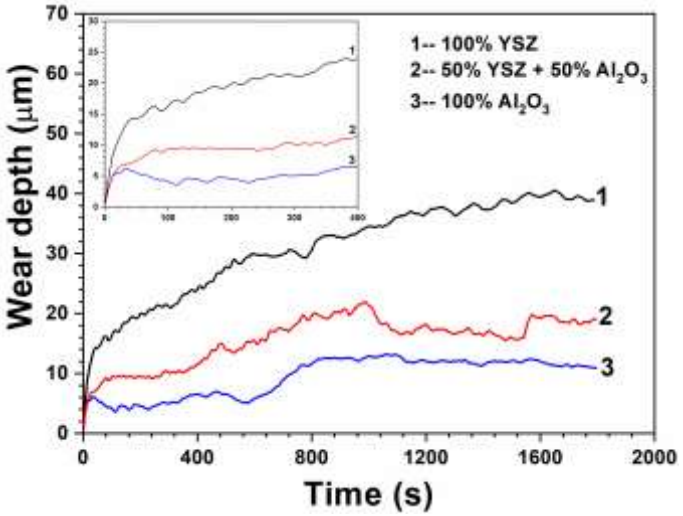

Fig. 6 Variation of wear depth with time in 100% YSZ coating (plot 1), 50% YSZ + 50% Al_2O_3 composite coating (plot 2) and 100% Al_2O_3 coating (plot 3) under 10 N load against WC ball. The early stage wear behaviour of the composite coating is shown in the same graph.

Fig. 7 shows the variation in the COF with time for the 100% YSZ coating (plot 1), 50% YSZ + 50% Al_2O_3 composite coating (plot 2), and 100% Al_2O_3 coating (plot 3) against WC ball measured using linear reciprocating wear at an applied normal load of 10 N. The 100% YSZ coating showed a high steady-state COF (~ 0.49) than 100% Al_2O_3 coating (~ 0.36) and 50% YSZ + 50% Al_2O_3 composite coating (~ 0.36). Higher COF in 100% YSZ coating was due to the abrasion action of loose WC and YSZ particles during a three-body abrasion process. An identical steady-state COF was measured for 100% Al_2O_3 and 50%

YSZ + 50% Al_2O_3 composite coatings. However, the steady-state COF in 100% Al_2O_3 coating was the lowest at the beginning which was due to 100 % Al_2O_3 coating being the hardest. The lower COF value in the 50% YSZ + 50% Al_2O_3 composite coating was believed to be due to higher fracture toughness of 50% YSZ + 50% Al_2O_3 composite coating which resulted in less debris formation.

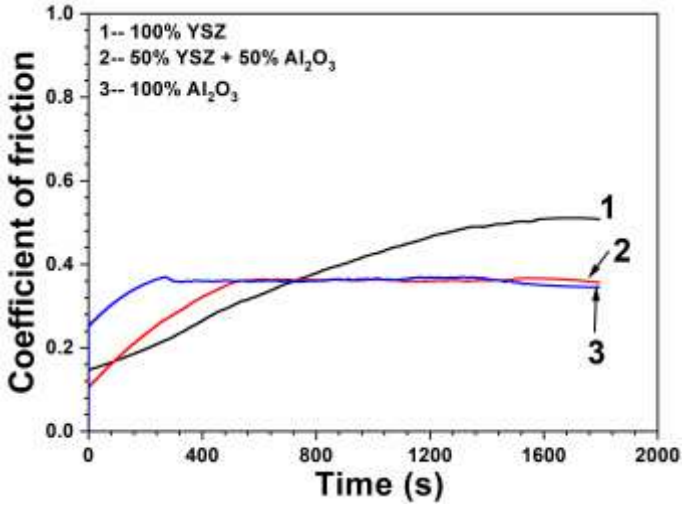

Fig. 7 Variation of COF with time in 100% YSZ coating (plot 1), 50% YSZ + 50% Al_2O_3 composite coating (plot 2) and 100% Al_2O_3 coating (plot 3) under 10 N load against WC ball.

Al_2O_3-CoNiCrAlY composite coating system

Fig. 8 shows the kinetics of wear in terms of variation of cumulative wear depth with time for the 100% Al_2O_3 coating (plot 1), 50% Al_2O_3 + 50% CoNiCrAlY composite coating (plot 2), and 100% CoNiCrAlY coating (plot 3) under a normal load of 10 N load against WC mating surface. The 100% Al_2O_3 and 100% CoNiCrAlY composite coatings showed a maximum wear resistance (lowest wear depth) as compared to 50% Al_2O_3 + 50% CoNiCrAlY composite coating as shown in Fig. 8. The superior wear resistance of 100% Al_2O_3 coating was due to its high hardness as compared to 50% Al_2O_3 + 50% CoNiCrAlY composite coating. The 100% CoNiCrAlY coating showed identical wear resistance as of 100% Al_2O_3 coating. The observed lowest wear rate in 100% CoNiCrAlY coating is believed to be due to the denser and tougher nature of the 100% CoNiCrAlY coating.

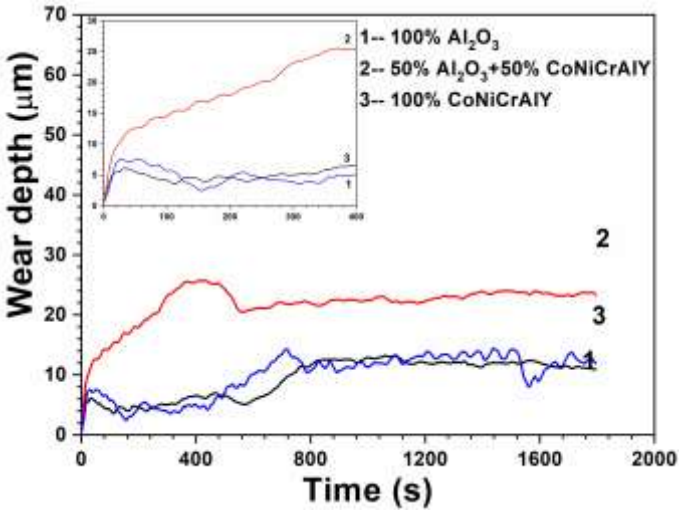

Fig. 8 Variation of wear depth with time in 100% Al_2O_3 coating (plot 1), 50% Al_2O_3 + 50% CoNiCrAlY composite coating (plot 2) and 100% CoNiCrAlY coating (plot 3) under 10 N load against WC ball. The earlystage wear behaviour of the composite coating is shown in the same graph.

Fig. 9 shows the variation in the COF with time for the 100% Al_2O_3 coating (plot 1), 50% Al_2O_3 + 50% CoNiCrAlY composite coating (plot 2), and 100% CoNiCrAlY coating (plot 3) under the applied normal load of 10 N. From Fig. 9, it may be noted that the 100% Al_2O_3 coating showed the lowest steady-state COF (~ 0.36) followed by 50% Al_2O_3 + 50% CoNiCrAlY composite coating (~ 0.43) and 100% CoNiCrAlY coating (~ 0.53). The lower steady-state COF in 100% Al_2O_3 coating was attributed to the higher hardness of the Al_2O_3 coating. The lower steady-state COF in 50% Al_2O_3 + 50% CoNiCrAlY composite coating over 100% CoNiCrAlY coating may be attributed to the formation of softer wear debris at the interface between the coating surface and WC ball which acts as a solid lubricant to reduce the COF.

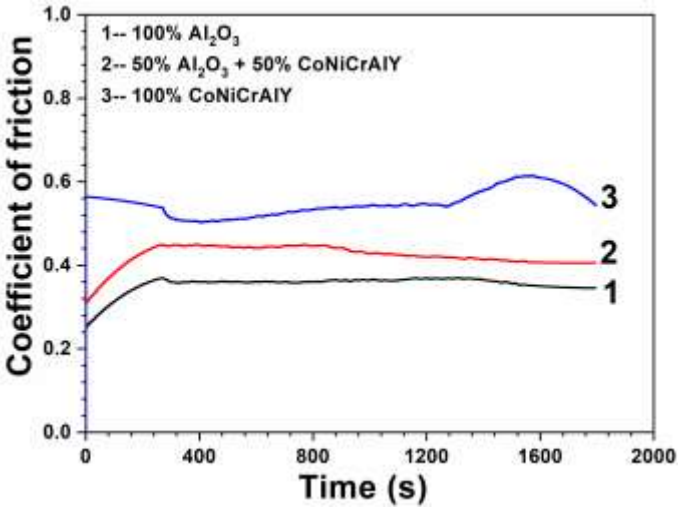

Fig. 9 Variation of COF with time in 100% Al_2O_3 coating (plot 1), 50% Al_2O_3 + 50% CoNiCrAlY coating (plot 2) and 100% CoNiCrAlY coating (plot 3) coatings under 10 N load against WC ball.

3.4. Post-wear analysis

Fig. 10 shows the scanning electron micrographs of the worn-out surface of 100% YSZ coating at (a) low magnification and the high magnification view of the same (b, c) under the applied normal load of 10 N. The adhesive wear mechanism was predominant in 100% YSZ coating. The brittleness of 100% YSZ coating along with higher porosity content resulted in the formation of many microcracks in the worn-out surface. The pre-existing defects in the 100% YSZ coating resulted in the aggravated plastic deformation of the YSZ splats followed by material removal. Localized particle pull-outs can also be evident from Fig. 10 (b) which are due to the presence of unmelted or partially melted powder particles as defects in the coating. The presence of hard debris is also evident from Fig. 10 (c). Fig. 11 shows the energy-dispersive X-ray spectroscopy (EDS) analysis of the wear debris formed in the worn-out surface of (a) 100% YSZ coating, (b) 50% YSZ + 50% CoNiCrAlY composite coating, (c) 100% CoNiCrAlY coating, (d) 50% YSZ + 50% Al_2O_3 composite coating, (e) 100% Al_2O_3 coating and (f) 50% Al_2O_3 + 50% CoNiCrAlY composite coating under 10 N load against WC ball. From Fig. 11 (a), the compositional analysis of 100% YSZ coating showed that the wear debris was mainly YSZ particles with some WC. These wear debris resulted in the increase in the COF in 100% YSZ coating.

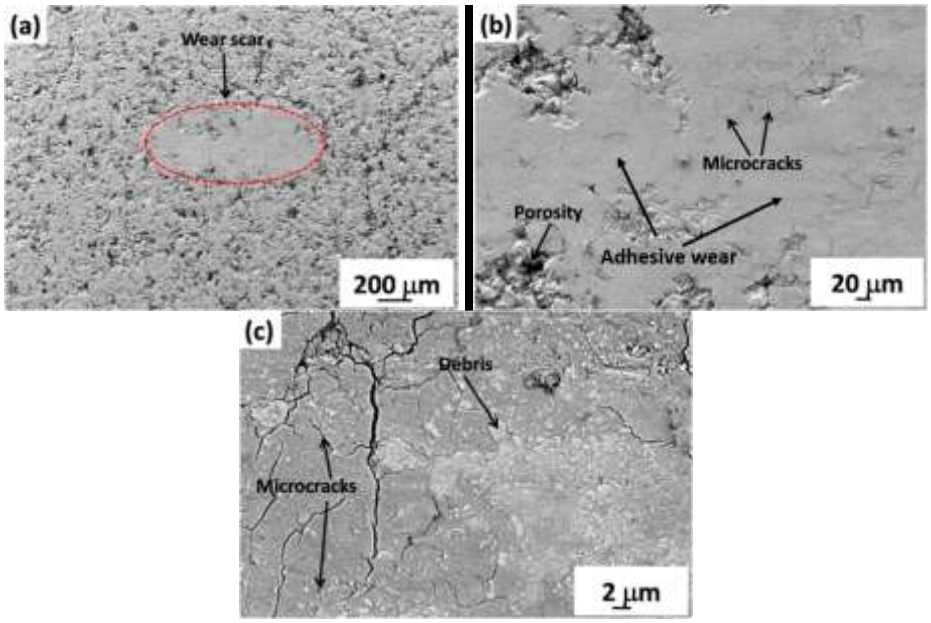

Fig. 10 Scanning electron micrograph of the worn-out surface of 100% YSZ coating under 10 N load against WC ball.

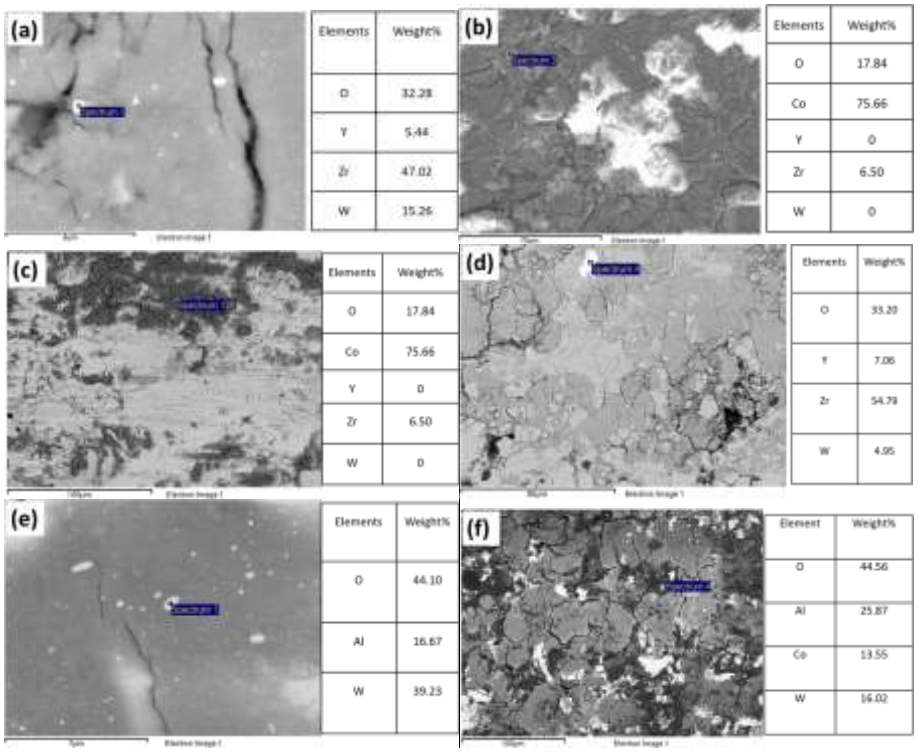

Fig. 11 Compositional analysis of the wear debris formed on the worn-out surface of (a) 100% YSZ coating, (b) 50% YSZ + 50% CoNiCrAlY composite coating, (c) 100% CoNiCrAlY coating, (d) 50% YSZ + 50% Al_2O_3 composite coating, (e) 100% Al_2O_3 coating and (f) 50% Al_2O_3 + 50% CoNiCrAlY composite coating under 10 N load against WC ball.

Fig. 12 shows the scanning electron micrographs of the worn-out surface of 50% YSZ + 50% CoNiCrAlY composite coating at (a) low magnification and (b) and (c) high magnification under the applied normal load of 10N. The worn-out surface showed the presence of microcracks and fractured splats. The pre-existing microcracks in the YSZ splats propagated under reciprocating load in a direction perpendicular to the coating-substrate interface. The propagating cracks led to a complete fracture of the splats due to abrasive and reciprocatory action of the WC ball. However, some areas near to deformed zone show less damage which is believed to be dominated by CoNiCrAlY phase. The adhesive wear mechanism was responsible for CoNiCrAlY patches. The presence of the metallic phase in the composite coating helped to slow down the crack propagation thereby reducing the wear rate. Fig. 11(b) shows the EDS compositional analysis of debris formed in the worn-out surface of 50% YSZ + 50% CoNiCrAlY composite coating. The analysis revealed that the loose debris was Co rich.

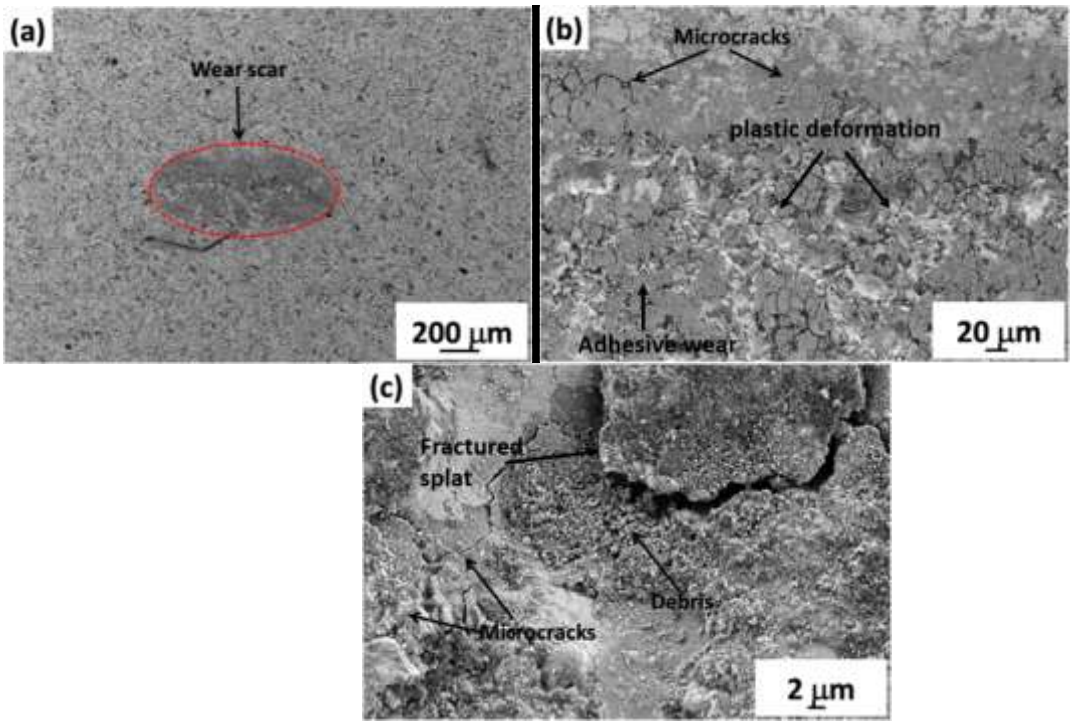

Fig. 12 Scanning electron micrograph of the worn-out surface of 50% YSZ + 50% CoNiCrAlY composite coating under 10 N load against WC ball.

Fig. 13 shows the scanning electron micrographs of the worn-out surface of 100% CoNiCrAlY coatings at low magnification and (b) and (c) at higher magnifications. As evident from Fig. 13, the worn-out surface showed fewer microcracks as a result of tougher 100% CoNiCrAlY coating. Fig. 13 (b) shows grooves and scratches on the worn-out surface which is due to abrasive action of WC counter-body. Formation of debris in the worn-out surface is also evident from Fig. 13 (c). The abrasion action of WC on the surface of 100% CoNiCrAlY coating was responsible for the increase in COF of the 100% CoNiCrAlY coating. Fig. 11 (c) shows the EDS compositional analysis of debris formed in the worn-out surface of 100% CoNiCrAlY coating. The wear debris was found to be Co rich.

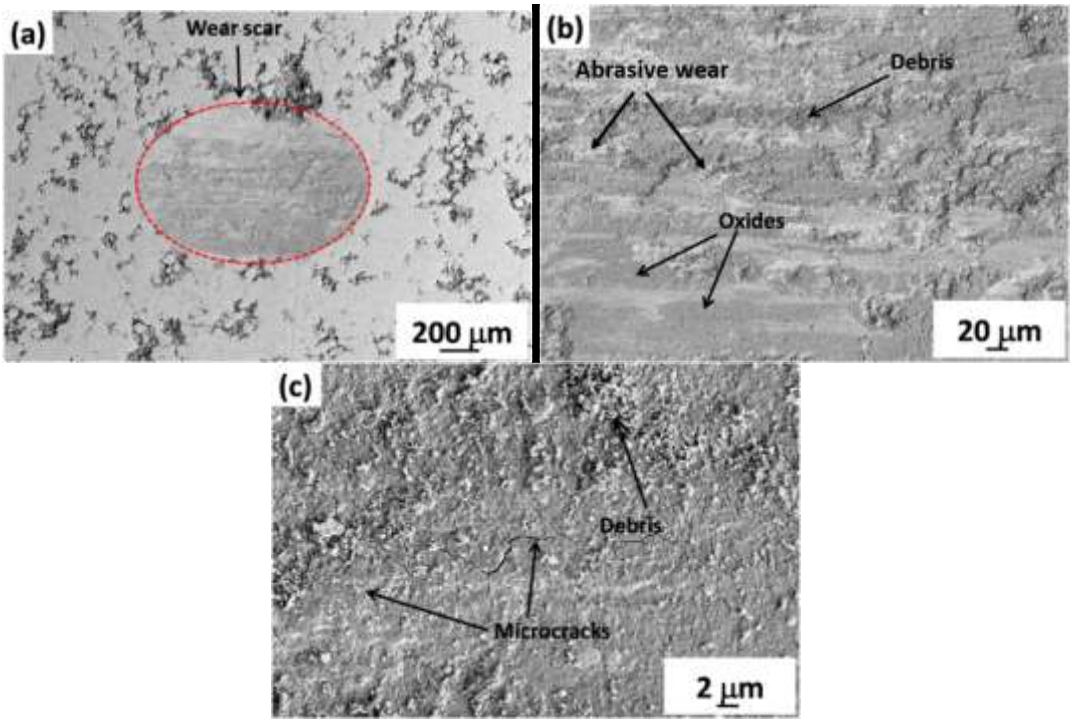

Fig. 13 Scanning electron micrograph of the worn-out surface of 100% CoNiCrAlY coating under 10 N load against WC ball.

Fig. 14 shows the scanning electron micrographs of 50% YSZ + 50% Al_2O_3 composite coating at (a) low magnification and (b) and (c) at high magnification. The microstructure of the worn-out surface showed high microcrack density. The higher density of microcracks in the worn-out surface is due to the presence

of brittle phases (YSZ and Al_2O_3) which plastically deformed under the action of reciprocating load. The microstructure of the worn-out surface revealed an adhesive wear mechanism as predominant. The propagation of cracks under the shear force acting on the surface led to the fracture of splats. The attachment of the worn-out material on to the surface due to adhesive wear is evident in Fig. 14 (c). The dark and light phases in the worn-out surface were Al_2O_3 and YSZ phases, respectively. The grey phase as marked by arrows was the bonded material due to adhesive wear. Fig. 11 (d) shows the EDS compositional analysis of debris formed in the worn-out surface of 50% YSZ + 50% Al_2O_3 composite coating. The analysis showed that the debris particles were YSZ. The presence of YSZ particles along the path of crack was found to slow down the crack propagation as shown in Fig. 14 (c). The slowing down of crack propagation led to reduced fracturing of splats which in turn slowed down the wear rate.

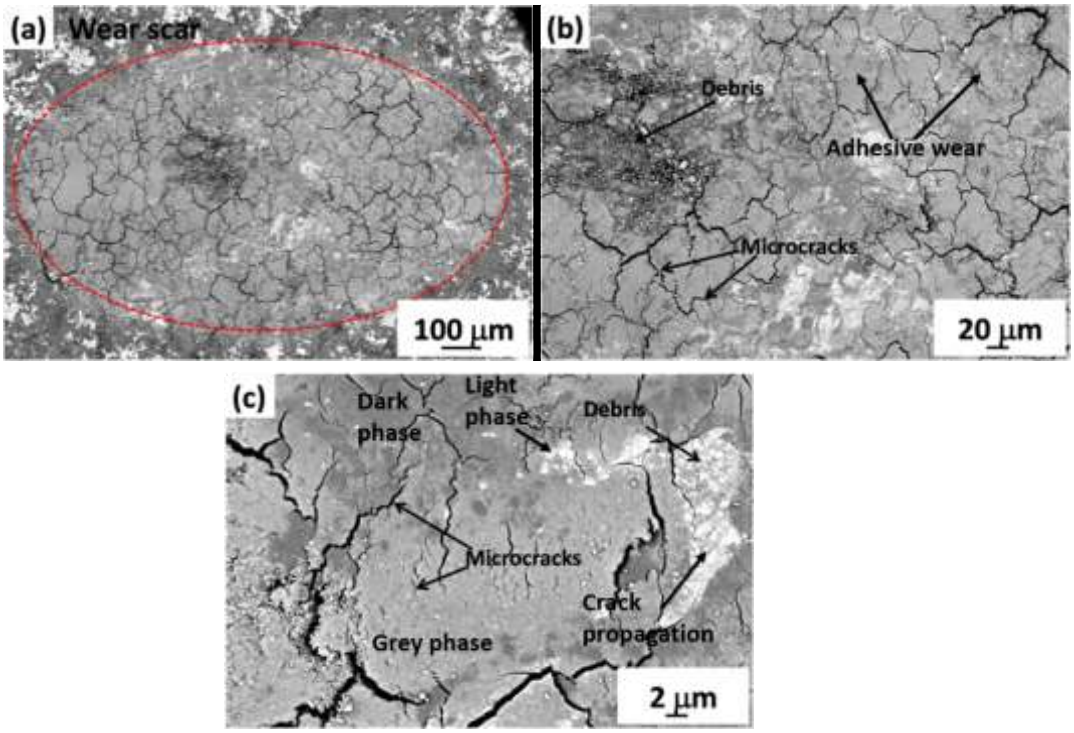

Fig. 14 Scanning electron micrograph of the worn-out surface of 50% YSZ + 50% Al_2O_3 composite coating under 10 N load against WC ball.

Fig. 15 shows the scanning electron micrographs of the worn-out surface of 100% Al_2O_3 coating at (a) low magnification and (b) and (c) high magnification under the applied normal load of 10 N. High density of microcracks can be seen in Fig. 15. The propagation of these microcracks under the influence of the

reciprocating load led to the fracture of Al_2O_3 splats. However, the severity of wear was less due to lower defect density and higher hardness of Al_2O_3 coating. The coating looked intact after the wear process implying strong bonding between splats. The wear debris formed in the worn-out surface of 100% Al_2O_3 coating was found to be rich in Al_2O_3 and WC as shown in Fig. 11 (e).

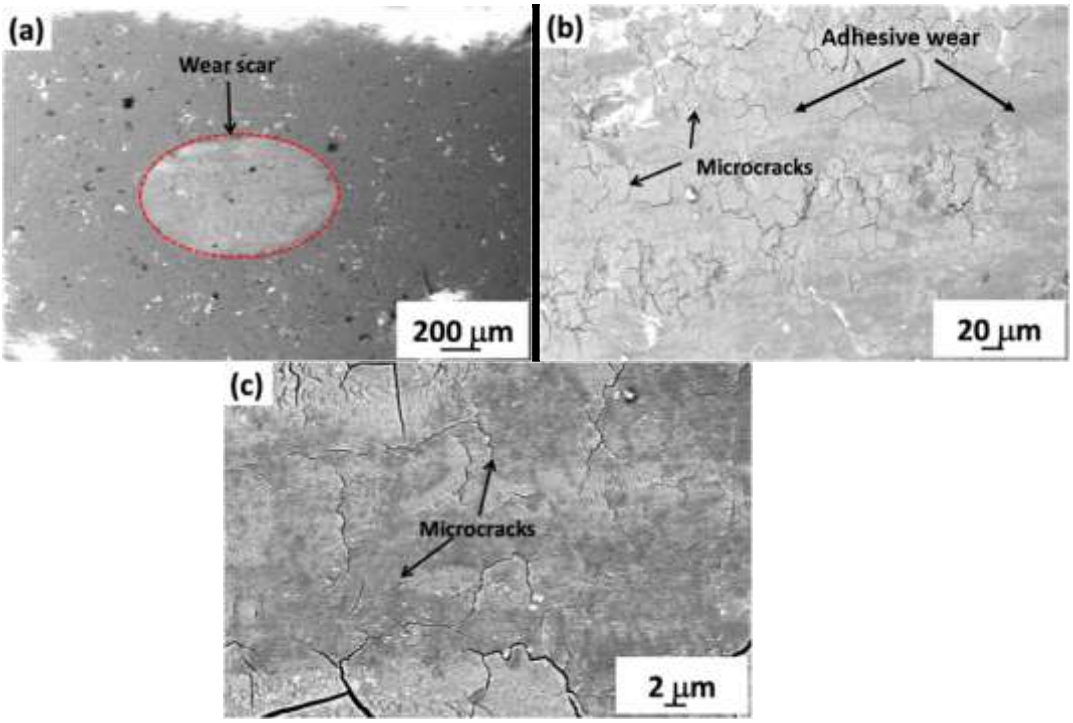

Fig. 15 Scanning electron micrograph of the worn-out surface of 100% Al_2O_3 coating under 10 N load against WC ball.

Fig. 16 shows the scanning electron micrographs of 50% Al_2O_3 + 50% CoNiCrAlY composite coating at (a) low magnification and (b) and (c) at high magnification under the applied load of 10 N. The plastic deformation of 50% Al_2O_3 + 50% CoNiCrAlY coating was severe under reciprocating load. The fracture of Al_2O_3 resulted in the formation of Al_2O_3 particles which were responsible for removal of softer CoNiCrAlY phase under high-stress abrasion. The EDS analysis of wear debris showed Al_2O_3 particles with WC as shown in Fig. 11 (f).

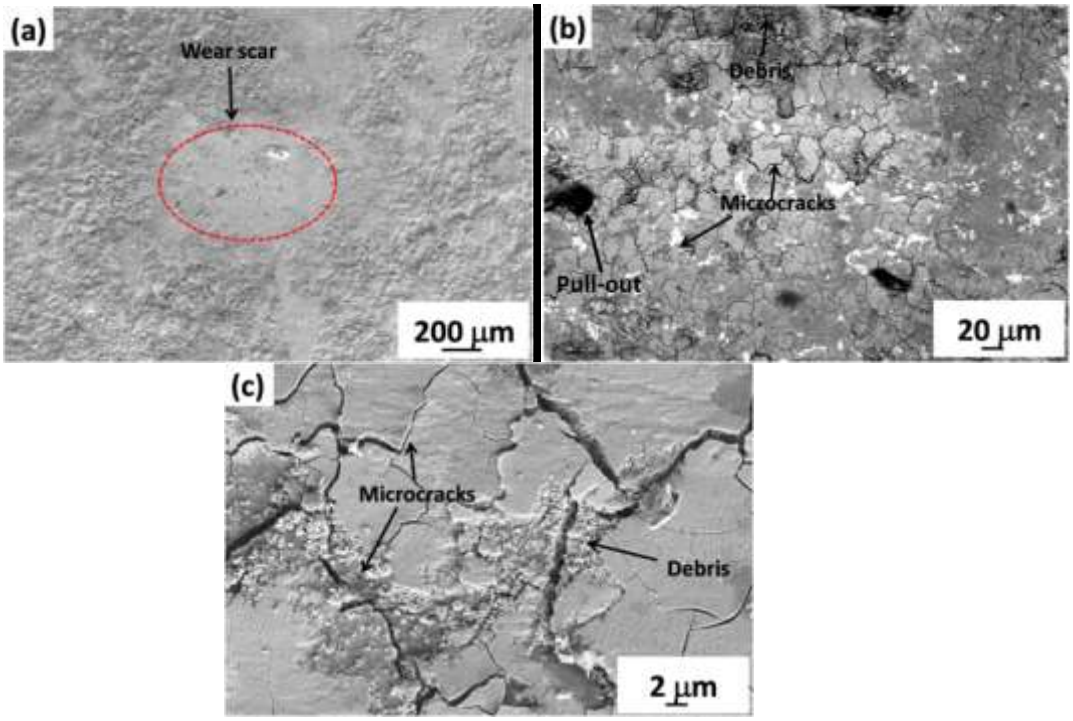

Fig. 16 Scanning electron micrograph of the worn-out surface of 50% Al_2O_3 + 50% CoNiCrAlY composite coating under 10 N load against WC ball.

Table 3 compares the tribological properties of the coatings in the present study with the reported literature. Table 3 includes studies with ball-on-disk sliding wear and ball-on-flat reciprocating wear. The applied load in the reported literature varies from 1 N to 80 N. The measured COF in the present study using a linear reciprocating wear tester at 10 N load was lower than most of the reported values. The measured COF values of 100% YSZ and 100% Al_2O_3 coatings was slightly higher than the reported value by Perumal *et al* [51] which was related to the specific wear mechanism. Perumal *et al* [51] reported a porosity 3.41% in YSZ coating and 2.42% in Al_2O_3 coating which was much lower than the measured values in the present study. The higher porosity in the present study acted as the stress concentration for crack propagation and formation of hard debris which increased the COF. The COF of the 50% YSZ + 50% Al_2O_3 composite coating was, however, comparable to the ZrO_2-60 wt.% Al_2O_3 composite coating [51]. The COF of the 50% YSZ + 50% Al_2O_3 composite coating was also much lower than the other YSZ and Al_2O_3 composite coatings as shown in Table 3. The observed difference was mainly due to the difference in the applied load, type of mating surface and porosity content in the coating.

Table 3 Comparison of the reported tribological properties of the coatings with the present study.

Coating materials	Wear test	Normal load	COF	Wear mechanism	Ref.
100% YSZ	Ball-on-flat linear reciprocating wear	10 N	0.49	Adhesive wear, microcracks, fracture of splats and pullouts	Present study
50% YSZ + 50% CoNiCrAlY			0.37	Mixed-mode wear, microcracks, severe plastic deformation and fracture of splats	
50% YSZ + 50% Al_2O_3			0.36	Adhesive wear, microcracks, deformation bands and fracture of splats	
100% Al_2O_3			0.36	Adhesive wear, microcracks and fracture of splats	
50% Al_2O_3 + 50% CoNiCrAlY			0.43	Adhesive wear, microcracks, grooves and severe plastic deformation	
100% CoNiCrAlY			0.53	Abrasive wear, grooves and microcracks	
8YSZ coating	Reciprocating ball-on-disk sliding wear	80 N	0.82	Plastic deformation and fracture of lamellae.	[22]
ZrO_2-71 wt% Al_2O_3 composite coating			0.62		
ZrO_2-15 vol% Al_2O_3 composite coating	Ball-on-disk sliding wear	5 N	0.7	Interfacial fatigue and brittle fracture of splats	[29]
ZrO_2-30 vol% Al_2O_3 composite coating			0.7	Ploughing and brittle fracture of splats	
8YSZ coating	Reciprocating ball-on-disk sliding wear	2 N	0.5–0.8	NA	[28]
8YSZ coating	Ball-on-disk sliding wear	10 N	0.7	Adhesive wear, spallation and brittle fracture of lamellae	[30]
8YSZ coating	Ball-on-disk sliding wear	20 N	2.1	Brittle fracture pf splats and abrasive wear	[31]
8YSZ coating	Ball-on-disk sliding wear	5 N	0.6	Plastic deformation, groove formation, intergranular fracture of splats	[34]
Al_2O_3 coating	Pin-on-disk sliding wear	5 N	0.87	Brittle fracture of splats	[35]
Al_2O_3 coating	Pin-on-disk sliding wear	30 N	0.9	Adhesive wear, spallation, crack propagation, abrasive wear and brittle fracture of splats	[37]
Al_2O_3 coating	Pin-on-disk	2 N	0.38	NA	[38]

	sliding wear				
ZrO_2- 25 wt% Al_2O_3 composite coating			0.39		
Al_2O_3 coating	Reciprocating ball-on-flat sliding wear	2 N	0.7	Abrasive wear and brittle fracture of splats	[11]
ZrO_2–60 wt.% Al_2O_3 composite coating	Ball-on-disk sliding wear	1 N	0.85	Abrasive wear	[52]
Al_2O_3 (P) coating	Ball-on-flat sliding wear	10 N	0.55	Adhesive wear, brittle fracture and grain pull-out.	[53]
Al_2O_3 (S) coating			0.37	Adhesive wear, brittle fracture and grain pull-out.	
YSZ (S)-80 wt% Al_2O_3 (P) composite coating			0.47	Brittle fracture and grain pull-out.	
YSZ (S)-80 wt% Al_2O_3 (S) composite coating			0.31	Brittle fracture and grain pull-out.	
Al_2O_3 (P) coating	Ball-on-flat linear reciprocating wear	NA	0.21	Pitting, intergranular fracture and grain pull-out	[6]
Al_2O_3 (S) coating			0.34		
YSZ (S)-80 wt% Al_2O_3 (P) composite coating			0.24		
YSZ (S)-80 wt% Al_2O_3 (S) composite coating			0.36		
ZrO_2- 60 wt.% Al_2O_3 composite coating	Reciprocating ball-on-disk sliding wear	20 N	0.45	Spallation and brittle fracture.	[54]
Al_2O_3 coating	Block-on-ring sliding wear	50 N	0.98	brittle fracture within the splats and delamination between splats	[55]
Al_2O_3 coating	Ball-on-plate reciprocating wear	10 N	0.31	Abrasive wear, grain pull-outs and brittle fracture of splats	[51]
8YSZ coating			0.41	Particle delamination	

ZrO_2- 60 wt.% Al_2O_3 composite coating			0.34	Microchipping, grain pull-outs and brittle fracture of splats	
Al_2O_3 coating	Pin-on-disk sliding wear	10 N	0.78	Adhesive wear and splats exfoliation	[56]

P- Powder feedstock; S- Suspension; NA- Not available

3.5. Mechanism of wear

Fig. 17 shows the three different stages of wear occurring during reciprocating wear of 100% CoNiCrAlY coating and ceramic coatings. During the onset of wear (stage I), the COF rose sharply for the metallic CoNiCrAlY and ceramic coatings. The increase in COF during stage I was attributed to the sudden increase in contact area due to micro-welding phenomena followed by plastic deformation of surface asperities under cyclic loading. The formation of powder bed acted as a third body and COF remained constant due to the balance between the rate of formation and removal of wear debris. During stage II wear of CoNiCrAlY coating, the micro-weld deformation occurred followed by the formation of soft loose particles which remained in the steady-state. In the third stage of wear in CoNiCrAlY coating, the oxidation of fine particles occurred due to frictional heating which increased the COF at the final stage. During stage II wear of ceramic coating, the deformation of micro-welds led to adhesive wear of the surface which increased the COF slowly or remained steady. At the final stage of wear (stage III), formation fine powder bed between the two surfaces acted as a third body which reduced the wear and brought a steady COF.

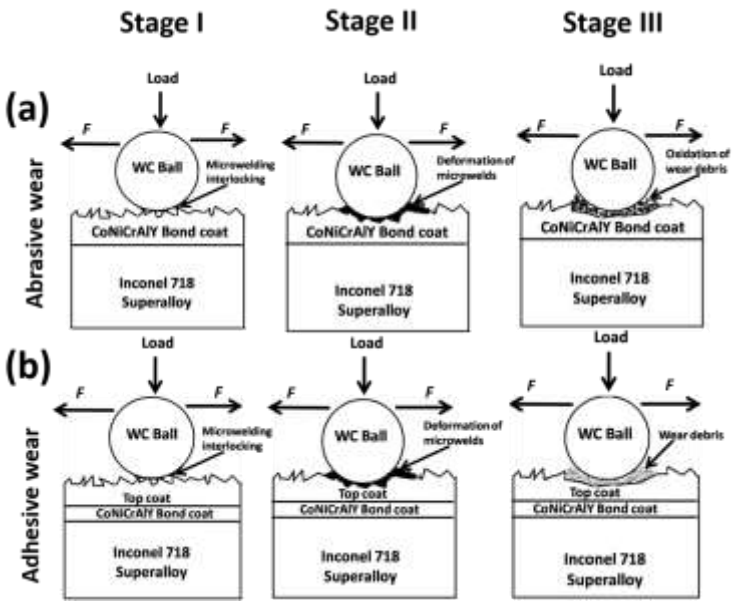

Fig. 22 Schematic representation showing the different stages in wear.

The deformation and wear performance of monolithic and composite coatings were different. During the wear of CoNiCrAlY coating, the material removal process was mostly dominated by abrasive wear. However, the wear mechanism in YSZ and Al_2O_3 coatings were adhesive wear with crack initiation and propagation leading to fracture of ceramic splats. The fracturing of splats was severe in 100% YSZ coating due to the presence of many microstructural defects. The high hardness of 100% Al_2O_3 coating along with comparatively lesser microstructural defects was resulted in less wear as compared to 100% YSZ coating. However, the presence of worn-out YSZ particles in the wear scar of the 50% YSZ + 50% Al_2O_3 composite coating resulted in the slowing down of microcrack propagation. Similarly, the microcrack propagation resistance was also increased by the presence of softer and tougher CoNiCrAlY phase in the 50% YSZ + 50% CoNiCrAlY composite coating.

4. Conclusions

In the present study, a detailed investigation of the linear reciprocating wear behaviour of YSZ based composite coatings was carried out. Wear and friction behaviour of the composite coatings were analysed

with varying composition of constituent phases. From the detailed investigation the following conclusions may be drawn:

1. The microhardness distribution in different coating systems was composition dependent. At the surface of CoNiCrAlY/Al_2O_3/YSZ composite coating, a microhardness of ~ 650 VHN was measured which gradually increased to ~ 1050 VHN for the 100% Al_2O_3 coating.

2. The linear reciprocating wear study showed the maximum wear resistance of the 100% Al_2O_3 and 100% CoNiCrAlY coatings. Having a harder and/or tougher phase on the surface showed significant improvement in the wear resistance. CMC coatings showed significant improvement in wear resistance as compared to monolithic ceramic coatings. The presence of 100% YSZ phase on the outer layer showed the lowest resistance to wear.

3. Maximum COF of ~ 0.53 was measured for 100% CoNiCrAlY coating amongst all the studied coatings. The 100% YSZ coating showed a COF value of ~ 0.5 and the 100% Al_2O_3 coating showed a COF of ~ 0.36. For the 50% YSZ + 50% CoNiCrAlY composite coating, a COF of ~ 0.36 was measured, whereas for the 50% Al_2O_3 + 50% CoNiCrAlY composite coating a COF of 0.43 was measured. Hardness and toughness of the composite coatings were found to be responsible for lowering the COF of the coatings.

4. Microcracks propagation and fracture of splats were responsible for the wear of ceramic phases and/or coatings. Adhesive wear was the predominant mechanism of wear in the ceramic coatings. Abrasive wear was the predominant mechanism of wear in metallic phases and/or coatings. In the 50% YSZ + 50% CoNiCrAlY and 50% Al_2O_3 + 50% CoNiCrAlY composite coatings, high-stress abrasion was the dominant wear mechanism.

5. Hardness and defect content in the coatings were found to affect the wear resistance and coefficient of friction of the coatings.

Acknowledgements

The authors acknowledge the partial financial support from the Department of Science and Technology (DST), New Delhi, Science and Engineering Research Board (under IMPRINT-II, Ref. No.: IMP/2018/001162/AM (Ver-1)), Indian Space Research Organization (ISRO), and Council of Scientific and Industrial Research (CSIR: 9/81(1170)/12 EMR-I), New Delhi.

Conflicts of interest

The authors declare that they have no conflict of interest.

References

[1] Y. Sun, B. Li, D.Q. Yang, T. Wang, Y. Sasaki, K. Ishii, Unlubricated friction and wear behaviour of zirconia ceramics, Wear., 1998, 215, p 232-236. https://doi.org/10.1016/S0043-1648(97)00247-0.

[2] R.H.J. Hannink, M.J. Murray, H.G. Scott, Friction and wear of partially stabilized zirconia: Basic science and practical applications, Wear., 1984, 100, p 355-366. https://doi.org/10.1016/0043-1648(84)90021-8.

[3] P. Ganapathy, G. Manivasagam, A. Rajamanickam, A. Natarajan, Wear studies on plasma–sprayed Al_2O_3 and 8mole% of yttrium–stabilized ZrO_2 composite coating on biomedical Ti–6Al–4V alloy for orthopedic joint application, Int. J. Nanomedicine. (2015). https://doi.org/10.2147/IJN.S79997.

[4] K.M. Reddy, A. Mukhopadhyay, B. Basu, Microstructure-mechanical-tribological property correlation of multistage spark plasma sintered tetragonal ZrO_2, J. Eur. Ceram. Soc., 2010, 30, p 3363-3375. https://doi.org/10.1016/j.jeurceramsoc.2010.08.005.

[5] X.Q. Cao, R. Vassen, D. Stoever, Ceramic materials for thermal barrier coatings, J. Eur. Ceram. Soc., 2004, 24, p 1-10. https://doi.org/10.1016/S0955-2219(03)00129-8.

[6] V. Gopal, S. Goel, G. Manivasagam, S. Joshi, Performance of hybrid powder-suspension axial plasma sprayed Al_2O_3-YSZ coatings in bovine serum solution, Materials., 2019, 12, p 1-18. https://doi.org/10.3390/ma12121922.

[7] B. Kerkwijk, A.J.A. Winnubst, H. Verweij, E.J. Mulder, H.S.C. Metselaar, D.J. Schipper, Tribological properties of nanoscale alumina-zirconia composites, Wear., 1999, 225/229, p 1293-1302. https://doi.org/10.1016/S0043-1648(98)00403-7.

[8] J. Chevalier, A.H. De Aza, G. Fantozzi, M. Schehl, R. Torrecillas, Extending the lifetime of ceramic orthopaedic implants, Adv. Mater., 2000, 12, p 1619-1621. https://doi.org/10.1002/1521-4095(200011)12:21<1619::AID-ADMA1619>3.0.CO;2-O.

[9] F. Kern, P. Palmero, Microstructure and mechanical properties of alumina 5 vol% zirconia

nanocomposites prepared by powder coating and powder mixing routes, Ceram. Int., 2013, 39, p 673-682. https://doi.org/10.1016/j.ceramint.2012.06.078.

[10] A. Perrichon, B. Liu, J. Chevalier, L. Gremillard, B. Reynard, F. Farizon, J.-D. Liao, J. Geringer, Ageing, shocks and wear mechanisms in ZTA and the long-term performance of hip joint materials, Materials (Basel)., 2017, 10, p 569-584. https://doi.org/10.3390/ma10060569.

[11] S.T. Aruna, N. Balaji, J. Shedthi, V.K.W. Grips, Effect of critical plasma spray parameters on the microstructure, microhardness and wear and corrosion resistance of plasma sprayed alumina coatings, Surf. Coatings Technol., 2012, 208, p 92-100. https://doi.org/10.1016/j.surfcoat.2012.08.016.

[12] R. V. Mangalaraja, B.K. Chandrasekhar, P. Manohar, Effect of ceria on the physical, mechanical and thermal properties of yttria stabilized zirconia toughened alumina, Mater. Sci. Eng. A., 2003, 343, p 71-75. https://doi.org/10.1016/S0921-5093(02)00368-4.

[13] T. Rodriguez-Suarez, J.F. Bartolomé, J.S. Moya, Mechanical and tribological properties of ceramic/metal composites: A review of phenomena spanning from the nanometer to the micrometer length scale, J. Eur. Ceram. Soc., 2012, 32, p 3887-3898. https://doi.org/10.1016/j.jeurceramsoc.2012.06.026.

[14] A.Z.A. Azhar, M.M. Ratnam, Z.A. Ahmad, Effect of Al_2O_3/YSZ microstructures on wear and mechanical properties of cutting inserts, J. Alloys Compd., 2009, 478, p 608-614. https://doi.org/10.1016/j.jallcom.2008.11.156.

[15] B. Smuk, M. Szutkowska, J. Walter, Alumina ceramics with partially stabilized zirconia for cutting tools, J. Mater. Process. Technol., 2003, 133, p 195-198. https://doi.org/10.1016/S0924-0136(02)00232-7.

[16] S.R. Choi, N.P. Bansal, Flexure strength, fracture toughness, and slow crack growth of YSZ/alumina composites at high temperatures, J. Am. Ceram. Soc., 2005, 88, p 1474-1480. https://doi.org/10.1111/j.1551-2916.2005.00252.x.

[17] G.. Liu, H.. Qiu, R. Todd, R.. Brook, J.. Guo, Processing and mechanical behavior of Al_2O_3/ZrO_2 nanocomposites, Mater. Res. Bull., 1998, 33, p 281–288. https://doi.org/10.1016/S0025-5408(97)00221-3.

[18] C.C. Berndt, J.H. Yi, The manufacture and microstructure of fiber-reinforced thermally sprayed coatings, Surf. Coatings Technol. 1989, 37, p 89-110. https://doi.org/10.1016/0257-8972(89)90123-0.

[19] J. Gao, Y. He, W. Gao, Fiber-reinforced yttria partially stabilized zirconia thermal barrier coatings processed by sol-gel method, High Temp. Mater. Process. 2011, 30, p 289–296. https://doi.org/10.1515/HTMP.2011.047.

[20] A.H. Pakseresht, M. Saremi, H. Omidvar, M. Alizadeh, Micro-structural study and wear resistance of thermal barrier coating reinforced by alumina whisker, Surf. Coatings Technol., 2019, 366, p 338-348 . https://doi.org/10.1016/j.surfcoat.2019.03.059.

[21] C. Wang, X. Cui, G. Jin, Z. Gao, J. Jin, Z. Cai, Y. Fang, Ceramic Fibers Reinforced Functionally Graded Thermal Barrier Coatings, Adv. Eng. Mater. 2017, 19, p 1700149. https://doi.org/10.1002/adem.201700149.

[22] H.S. Ahn, J.Y. Kim, D.S. Lim, Tribological behaviour of plasma-sprayed zirconia coatings, Wear., 1997, 203/204, p 77-87. https://doi.org/10.1016/S0043-1648(96)07395-4.

[23] M.H. Ghaemi, S. Reichert, A. Krupa, M. Sawczak, A. Zykova, K. Lobach, S. Sayenko, Y. Svitlychnyi, Zirconia ceramics with additions of Alumina for advanced tribological and biomedical applications, Ceram. Int., 2017, 43, p 9746-9752. https://doi.org/10.1016/j.ceramint.2017.04.150.

[24] Y.J. He, A.J.A. Winnubst, D.J. Schipper, A.J. Burggraaf, H. Verweij, Effects of a second phase on the tribological properties of Al_2O_3 and ZrO_2 ceramics, Wear., 1997, 210, p 178187. https://doi.org/10.1016/S0043-1648(96)07515-1.

[25] Y. Fang, N. Chen, G. Du, M. Zhang, X. Zhao, J. Wu, Effect of Y_2O_3-stabilized ZrO_2 whiskers on the microstructure, mechanical and wear resistance properties of Al_2O_3 based ceramic composites, Ceram. Int., 2019, 45, p 16504-16511. https://doi.org/10.1016/j.ceramint.2019.05.184.

[26] R.J.L. Steenbakker, R.G. Wellman, J.R. Nicholls, Erosion of gadolinia doped EB-PVD TBCs, Surf. Coating Technol., 2006, 201, p 2140-2146 . https://doi.org/10.1016/j.surfcoat.2006.03.022.

[27] R.G. Wellman, J.R. Nicholls, K. Murphy, Effect of microstructure and temperature on the erosion rates and mechanisms of modified EB-PVD TBCs, Wear., 2007, 267, p 19271934. https://doi.org/10.1016/j.wear.2009.04.002.

[28] S.T. Aruna, N. Balaji, K.S. Rajam, Phase transformation and wear studies of plasma sprayed yttria stabilized zirconia coatings containing various mol% of yttria, Mater. Charact., 2011, 62, p 697-705 . https://doi.org/10.1016/j.matchar.2011.04.018.

[29] B. Liang, G. Zhang, H. Liao, C. Coddet, C. Ding, Friction and wear behavior of ZrO_2-Al_2O_3 composite coatings deposited by air plasma spraying: Correlation with physical and mechanical properties, Surf. Coatings Technol., 2009, 203, p 3235-3242. https://doi.org/10.1016/j.surfcoat.2009.03.056.

[30] J.F. Li, H. Liao, X.Y. Wang, B. Normand, V. Ji, C.X. Ding, C. Coddet, Improvement in wear resistance of plasma sprayed yttria stabilized zirconia coating using nanostructured powder, Tribol. Int., 2004, 37, p 77-84. Tribol. Int. (2004). https://doi.org/10.1016/S0301-679X(03)00138-5.

[31] H. Chen, Y. Zhang, C. Ding, Tribological properties of nanostructured zirconia coatings deposited by plasma spraying, Wear., 2002, 253, p 885-893. https://doi.org/10.1016/S0043-1648(02)00221-1.

[32] Y. Zeng, S.W. Lee, L. Gao, C.X. Ding, Atmospheric plasma sprayed coatings of nanostructured zirconia, J. Eur. Ceram. Soc., 2002, 22, p 347-351. https://doi.org/10.1016/S0955-2219(01)00291-6.

[33] H. Chen, C.X. Ding, Nanostructured zirconia coating prepared by atmospheric plasma spraying, Surf. Coatings Technol., 2002, 150, p 31-36. https://doi.org/10.1016/S0257-8972(01)01525-0.

[34] S. Tao, B. Liang, C. Ding, H. Liao, C. Coddet, Wear characteristics of plasma-sprayed nanostructured yttria partially stabilized zirconia coatings, J. Therm. Spray Technol., 2005, 14, p 518-523. https://doi.org/10.1361/105996305X76540.

[35] G. Bolelli, V. Cannillo, L. Lusvarghi, T. Manfredini, Wear behaviour of thermally sprayed ceramic oxide coatings, Wear., 2006, 261, p 1298-1315. https://doi.org/10.1016/j.wear.2006.03.023.

[36] H.S. Ahn, O.K. Kwon, Wear behaviour of plasma-sprayed partially stabilized zirconia on a steel substrate, Wear., 1993, 162/164, p 636-644. https://doi.org/10.1016/0043-1648(93)90556-2.

[37] V.P. Singh, A. Sil, R. Jayaganthan, A study on sliding and erosive wear behaviour of atmospheric plasma sprayed conventional and nanostructured alumina coatings, Mater. Des., 2011, 32, p 584-591. https://doi.org/10.1016/j.matdes.2010.08.019.

[38] O. Tingaud, P. Bertrand, G. Bertrand, Microstructure and tribological behavior of suspension plasma sprayed Al2O3 and Al2O3-YSZ composite coatings, Surf. Coatings Technol., 2010, 1004-1008. https://doi.org/10.1016/j.surfcoat.2010.06.003.

[39] N. Ramanujam, T. Nakamura, Erosion mechanisms of thermally sprayed coatings with multiple phases, Surf. Coatings Technol., 2009, 204, p 42-53. https://doi.org/10.1016/j.surfcoat.2009.06.024.

[40] D. Chen, E.H. Jordan, M. Gell, Microstructure of suspension plasma spray and air plasma spray Al_2O_3-ZrO_2 composite coatings, J. Therm. Spray Technol., 2009, 18, p 421–426. https://doi.org/10.1007/s11666-009-9306-5.

[41] Y. da Chen, Y. Yang, Z. hua Chu, X. guang Chen, L. Wang, Z. Liu, Y. chun Dong, D. ran Yan, J. xin Zhang, Z. long Kang, Microstructure and properties of Al_2O_3 -ZrO_2 composite coatings prepared by air plasma spraying, Appl. Surf. Sci., 2018, 431, p 93-100. https://doi.org/10.1016/j.apsusc.2017.04.073.

[42] K. He, J.J. Chen, W.X. Weng, C.C. Li, Q. Li, Microstructure and mechanical properties of plasma sprayed Al2O3-YSZ composite coatings, Vacuum., 2018, 151, p 209-220. https://doi.org/10.1016/j.vacuum.2018.01.038.

[43] S. Nath, I. Manna, A.K. Jha, S.C. Sharma, S.K. Pratihar, J. Dutta Majumdar, Thermophysical behavior of thermal sprayed yttria stabilized zirconia based composite coatings, Ceram. Int., 2017, 43, p 11204-11217. https://doi.org/10.1016/j.ceramint.2017.05.170.

[44] S. Nath, I. Manna, J.D. Majumdar, Nanomechanical behavior of yttria stabilized zirconia (YSZ) based thermal barrier coating, Ceram. Int. 2015, 41, p 5247-5256. https://doi.org/10.1016/j.ceramint.2014.11.039.

[45] J. Ilavsky, A.J. Allen, G.G. Long, S. Krueger, C.C. Berndt, H. Herman, Influence of spray angle on the pore and crack microstructure of plasma-sprayed deposits, J. Am. Ceram. Soc., 1997, 80 (3), p 733-742 . https://doi.org/10.1111/j.1151-2916.1997.tb02890.x.

[46] S.-H. Leigh, C.C. Berndt, Quantitative evaluation of void distributions within a plasma-sprayed ceramic, J. Am. Ceram. Soc., 2004, 82, p 17-21. https://doi.org/10.1111/j.1151-2916.1999.tb01717.x.

[47] M. Xue, S. Chandra, J. Mostaghimi, H.R. Salimijazi, Formation of pores in thermal spray coatings due to incomplete filling of crevices in patterned surfaces, Plasma Chem. Plasma Process., 2007, 27, p 647-657 . https://doi.org/10.1007/s11090-007-9097-8.

[48] S. Stecura, Optimization of the NiCrAlY/ZrO_2/Y_2O_3 thermal barrier system, NASA-TM86905 (1985).

[49] K.A. Khor, Y.W. Gu, Z.L. Dong, Plasma spraying of functionally graded yttria stabilized zirconia/NiCoCrAlY coating system using composite powders, J. Therm. Spray Technol. 2000, 9, p 245-249. https://doi.org/10.1361/105996300770349999.

[50] Y. Wang, S.M. Hsu, Wear and wear transition mechanisms of ceramics, Wear. 1996, 195, p 112-122. https://doi.org/10.1016/0043-1648(95)06800-7.

[51] G. Perumal, M. Geetha, R. Asokamani, N. Alagumurthi, Wear studies on plasma sprayed Al_2O_3-40wt% 8YSZ composite ceramic coating on Ti-6Al-4V alloy used for biomedical applications, Wear., 2014, 311, 101-113. https://doi.org/10.1016/j.wear.2013.12.027.

[52] J. Suffner, H. Sieger, H. Hahn, S. Dosta, I.G. Cano, J.M. Guilemany, P. Klimczyk, L. Jaworska, Microstructure and mechanical properties of near-eutectic ZrO_2-60wt.% Al_2O_3 produced by quenched plasma spraying, Mater. Sci. Eng. A., 2009, 506, p 180-186. https://doi.org/10.1016/j.msea.2008.11.034.

[53] J.W. Murray, A. Leva, S. Joshi, T. Hussain, Microstructure and wear behaviour of powder and suspension hybrid Al_2O_3–YSZ coatings, Ceram. Int., 2018, 44, p 8498-8504. https://doi.org/10.1016/j.ceramint.2018.02.048.

[54] X. Zhao, Y. An, J. Chen, H. Zhou, B. Yin, Properties of Al_2O_3-40 wt.% ZrO_2 composite coatings from ultra-fine feedstocks by atmospheric plasma spraying, Wear., 2008, 265, p 1642-1648. https://doi.org/10.1016/j.wear.2008.03.019.

[55] Z. Yin, S. Tao, X. Zhou, C. Ding, Tribological properties of plasma sprayed Al/Al_2O_3 composite coatings, Wear. 2007, 263, p 1430-1437. https://doi.org/10.1016/j.wear.2007.01.052.

[56] P.P. Psyllaki, M. Jeandin, D.I. Pantelis, Microstructure and wear mechanisms of thermal-sprayed alumina coatings, Mater. Lett., 2001, 47, p 77-82. https://doi.org/10.1016/S0167-577X(00)00215-9.